# Kalman filter-driven state observer for thermal error compensation in machine tool digital twins

**Journal Article**

**Author(s):**
Lang, Sebastian Beat; Talleri, Sofia; Mayr, Josef; Wegener, Konrad; Bambach, Markus

**Publication date:**
2024-10

**Permanent link:**
https://doi.org/https://doi.org/10.3929/ethz-b-000700740



**Originally published in:**
Manufacturing Letters 41, https://doi.org/10.1016/j.mfglet.2024.09.025

Available online at www.sciencedirect.com

Manufacturing Letters

Manufacturing Letters 41 (2024) 208–218

52nd SME North American Manufacturing Research Conference (NAMRC 52, 2024)

# Kalman Filter-Driven State Observer for Thermal Error Compensation in Machine Tool Digital Twins

Sebastian Lang[a,b,*], Sofia Talleri[a], Josef Mayr[b], Konrad Wegener[b], Markus Bambach[a]

[a]*Advanced Manufacturing Lab ETH Zurich, Technoparkstrasse 1, 8005 Zurich, Switzerland*
[b]*inspire AG, Technoparkstrasse 1, 8005 Zurich, Switzerland*

**Abstract**

Sustainable reduction of thermal errors during production is the key challenge in modern high-precision manufacturing. Numerical compensation models provide an energy-efficient solution, but in the case of data-driven models, high-quality experimental data must be time-consuming and expensive to produce, negatively impacting overall productivity. Furthermore, robustness concerns arise in the case of new operating conditions, which were not contained in the training data. This paper presents a novel use of a Kalman filter together with model order reduced finite element models to observe the entire thermal state, which allows the subsequent solution of the mechanical model and computation of the thermal errors in real-time without requiring any training data but instead purely based on the physical system model. The effectiveness of this approach is evaluated using experiments on a thermal test bench with 16 out of 40 temperature sensors employed for observation and demonstrated on a 5-axis machine tool (MT) with 13 out of 25 temperature sensors used. Due to the combination of the reduced order model and Kalman filter these 13 temperature sensors are sufficient to represent a MT mesh of more than 350'000 elements. The entire temperature profile of the thermal test bench is reconstructed to achieve a root mean square error (RMSE) of the unobserved temperature sensors of only 2.7 $^\circ C$, which accounts for more than 83% of all temperature variations and 1.3 $^\circ C$ for the 5-axis MT. For the thermal error of the thermal test bench, the RMSE could be reduced from 67.4 $\mu m$ to 33.3 $\mu m$, corresponding to a reduction of 52.7 %. This could be achieved without the need for experimental data for model calibration, in a real-time capable physics-based model.



*Keywords:* Thermal errors ; Machine tools ; Kalman filter ; Digital twin ; Compensation

## 1. Introduction

Thermal errors in machine tools (MTs) are one of the most significant obstacles in precision manufacturing. According to Mayr et al. [25], thermal errors can cause up to 75% of geometric errors in machined workpieces. Reducing these errors in practice is still a difficult challenge since they are influenced by many internal and external heat sources, as described by Bryan [5]. Approaches for stabilizing the temperatures are often energy-intensive and require precise tempering of both the machine tool components [9] and the environment [28]. On the other hand, numerical compensation approaches aim to predict and mitigate thermal errors without additional energy expenditure. Numerical models used for compensation are usually either black box data-driven models or physics-based white box models such as Finite Element (FE) methods, and, in both cases, require very high robustness [26]. Numerical compensation approaches require a timely prediction of the current deformation which can be used to shift the tool center point (TCP) position using the MT control [23]. This is limited by the available computational power and model complexity. At the same time, training data for data-driven models is very time-consuming to generate and, therefore, expensive [7]. Accordingly, model architectures are typically designed to work with very little data. For example, Blaser et al. [4] show that a

* Corresponding author.
*E-mail address:* selang@ethz.ch (Sebastian Lang).

model update-enabled self-learning approach can continuously improve the compensation model, allowing the model to retrain and improve in case it performs poorly. Mayr et al. [24] extended this self-learning model by the use of training weights. Zimmermann et al. [35, 34] used adaptive input selection to modify the selected inputs once the model requires retraining. Lang et al. [21] used the power of the MT as a model input besides the temperature sensors and quantified the energy requirement of data-driven compensation models due to their training data requirements, which can be quickly in the hundreds to thousands of kWh and creates the need for data efficient or data less compensation approaches. Zimmermann et al. [37] demonstrated the use of thermal error compensation during the production of impeller workpieces, showing the real-world benefit of thermal error compensation and reducing the error on sensitive workpieces by more than 70%. Instead of discrete temperature sensors, thermal camera images have been successfully used in combination with deep learning by Chengyang et al. [6], or adaptive neuro-fuzzy inference system by Abdulshahed et al. [1]. However, these data-driven models are still limited by the availability and quality of their training data. Other approaches use more physics-based models, such as FE models.

Kalman filters are a common tool used in dealing with state space systems with many different applications [3]. For example Guo et al. [11] use it for planning the measurement process in geometric calibration of machine tools during assembly. Polotski et al. [30] use a Kalman filter for adaptive production control with imprecise demand and supply information. Kim et al. [18] use an infrared camera to monitor the thermal state during fused deposition modeling of additive manufacturing processes.

Digital twins can be used along the entire manufacturing value chain and see promising use in fusing simulations and process control and monitoring [22]. However, for this purpose full-scale computation of FE-models is rarely feasible. Therefore, computational efficiency has to be increased, such as provided by model order reduction approaches [15]. Gomez-Acedo et al. [10] used a Kalman filter and a lumped mass model of a machine tool with four states to achieve a physics-based compensation model. Kizaki et al. [20] placed 284 temperature sensors on a machine tool and applied linear interpolation in all three dimensions to obtain the temperature field of an FE-model generated using ANSYS. This allowed the subsequent solution of the mechanical model to calculate the thermal errors. However, such a high number of temperature sensors is not practical, and more information about the system behavior, such as conduction and convection properties and locations of heat sources, could be used to improve from linear interpolation.

To overcome the limitations, this paper presents a novel approach using Kalman filters to reconstruct the complete temperature field from a small number of sensors. Subsequent evaluation of the mechanical system yields the thermo-mechanical deformations that can compensate for the thermal errors in an MT.

The digital twin representation used for the MT and the thermal test bench is described in Section 2. Afterwards, Section 3 describes the structure of the Kalman filter, which is used to observe the entire reduced thermal space. Section 4 introduces the experimental setup of the thermal test bench and the 5-axis machine tool. Subsequently, Section 5 presents the results for the thermal test bench and a 5-axis machine tool and compares the predictions to measurements. Section 6 summarizes the developments and gives an outlook for future work.

Table 1: Model size of the FE-model and modes after reduction for all components of the thermal test bench and 5-axis MT .

| | | FE nodes | Reduced modes |
|---|---|---|---|
| **Thermal test bench** | **Frame** | 186’339 | 48 |
| | **Meas. Holder** | 22’602 | 8 |
| | **Total** | 208’941 | 56 |
| **5-axis MT** | **Ball screws** (X,2Y,2Z) | 48’850 | 80 |
| | **Bed** | 105’807 | 30 |
| | **Y-axis** | 34’119 | 50 |
| | **X-axis** | 40’693 | 20 |
| | **Z-axis** | 20’760 | 9 |
| | **Spindle** | 9’366 | 5 |
| | **B-axis** | 77’918 | 15 |
| | **C-axis** | 15’656 | 5 |
| | **Total** | 353’169 | 214 |

## 2. Thermomechanical digital twin model

This Section presents a modeling procedure and the model that is then applied and adapted to both machine tool and thermal test bench as a digital twin for thermal state estimation and subsequent thermal error compensation.

### 2.1. Setup of digital twin

In the first step, a CAD model of both systems is used to generate a FE mesh of each component using ANSYS. This can be exported using the software MORe [32, 12] to consider the mesh as a state space model for the thermal and mechanical system. This allows a downsize of the model to a reduced space using a Krylov Modal Subspace (KMS) reduction, which ensures accuracy in the frequency range of interest as described by Hernández-Becerro et al. [13] and Spescha et al. [31].

Table 1 shows the model size of the thermal model for both the thermal test bench and 5-axis MT. The thermo-mechanical model would contain a total of 469 modes for the 5-axis MT and 244 for the thermal test bench.

$$\mathbf{E}\dot{\mathbf{x}}(t) = \mathbf{A}\mathbf{x}(t) + \mathbf{B}\mathbf{u}(t) \tag{1}$$

A linear time-invariant (LTI) system is described in Equation 1. This can be used in a thermal system to represent a first order system of ordinary differential equations (ODE). In this case, $\mathbf{A}$ is the system matrix containing conduction and convection, $\mathbf{E}$ is the mass matrix containing the thermal capacity, $\mathbf{B}$ the input matrix, and $\mathbf{u}$ the input vector. $\mathbf{x}(t)$ is the thermal state of the system representing its temperatures. $\mathbf{u}$ is assumed to be zero as no knowledge about the system’s heat inputs is assumed. Measuring system’s heat inputs in a real production system is highly challenging.

The reaction to external changes and disturbances is registered through system changes at the measurement level, as the measurements can easily be executed at high frequencies compared to the slow thermal changes in the system. The physical parameters of the system, such as material properties or heat transfer coefficients of convective surfaces, are assumed to be constant.

$$\mathbf{y}_{mech}(t) = \mathbf{C}_i\mathbf{K}^{-1}\mathbf{K}_{th}\mathbf{x}(t) \tag{2}$$

The mechanical part of the digital twin is represented by equation 2. $\mathbf{y}_{mech}(t)$ represents the mechanical deformation at time t. $\mathbf{C}_i$ is the mechanical link between different points: in the case of the thermal test bench this is between the displacement of the probe holder, representing the workpiece center point (WCP), and tool tip, representing the tool center point (TCP). $\mathbf{K}^{-1}$ is the mechanical stiffness matrix based on the material properties and mesh of the system. $\mathbf{K}_{th}$ is the coupling matrix between the thermal and mechanical system: it induces a volume force based on the thermal expansion coefficient $\alpha$.

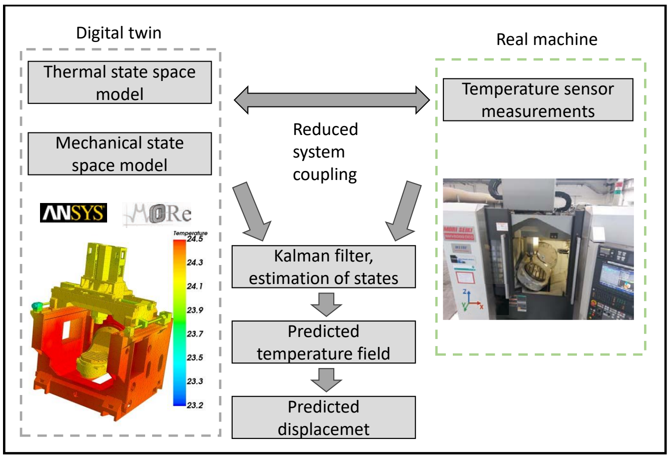


Figure 1: Concept of the use of the Kalman filter together with the digital twin of the machine tool to allow thermal error prediction.

Figure 1 summarizes the concept of the Kalman filter based thermal error compensation. In order to prevent extensive computation or system model requirements, the thermal field is observed with the help of the Kalman filter and a number of temperature sensors.

## 2.2. Discretization

The previously mentioned LTI system is a continuous representation of a system that can only be observed using temperature in discrete time. Therefore, a discretization must be carried out to apply a Kalman filter to the system [27]. The sampling rates are in the range of 2.5 to 10 seconds, which is very fast compared to the slower-acting thermal errors. Zero order hold, first order hold (assuming piecewise linear inputs) and impulse invariant discretization methods all perform almost identically.

## 2.3. Input selection

To select the input sensors for the Kalman filter, k-means clustering [29] with z-score normalization is utilized. Input selection of the observed sensors is essential as otherwise collinear inputs and measurement noise can lead to numeric instability ( as happens in regression models used in thermal error compensation [35]). For this reason, a clustering of the links between each sensor's observed states (**C**) is performed, and the sensor closest, in a square Euclidean representation, to each cluster location is selected. This is repeated with a growing number $k$ of sensors used for clustering, until either the system is fully observable or the selected maximum number of temperature sensors is reached. This is the case for the 5-axis MT as not all moving components, such as the ball screws, can have their temperature measured with reasonable effort. The system of 5-axis MT is therefore not fully observable even if all installed sensors would be used.

# 3. Kalman filter methodology

In this Section, the approach for state estimation based on Kalman filter is described [17].

## 3.1. Overview

A Kalman filter is a recursive estimation algorithm that allows the reconstruction of dynamical systems' state variables based on few noisy measurements. Specifically, a discrete Kalman filter is used here to correlate measurements from temperature sensors to the states of the thermal system in the reduced domain so that a prediction for the evolution of dynamic states and, consequently, of the temperature field can be obtained. The used modeling flow is shown in Figure 2.

$$\mathbf{x}(k) = \mathbf{A}\cdot\mathbf{x}(k-1) + \mathbf{B}\cdot\mathbf{u}(k-1) + \mathbf{v}(k-1) \tag{3}$$
$$\mathbf{z}(k) = \mathbf{H}\cdot\mathbf{x}(k) + \mathbf{w}(k) \tag{4}$$

with $\mathbf{x}(0) \sim \mathcal{N}(\mathbf{x}_0, \mathbf{P}_0)$, $\mathbf{w}(k) \sim \mathcal{N}(0, \mathbf{Q})$ process noise, $\mathbf{v}(k) \sim \mathcal{N}(0, \mathbf{R})$ sensor noise and $\mathbf{z}(k)$ being the measurements.

Equations 3 and 4 encompasses the formulation of a discrete linear time-invariant system in state space representation that allows the application of this algorithm. While Equation 3 describes the state update based on system dynamics and includes the zero-mean Gaussian process noise **v**, Equation 4 expresses the coupling of measurements and states through the observer matrix **H** to which the zero-mean Gaussian measurement noise **w** is added. The assumption of Gaussian noise is crucial for the theoretical derivation of the Kalman filter update equations. For this application the system model is derived from Equation 1 described in subsection 2.1.

The Kalman filter estimation method consists of two main stages: the a priori prediction step and the a posteriori measurement update step [2].

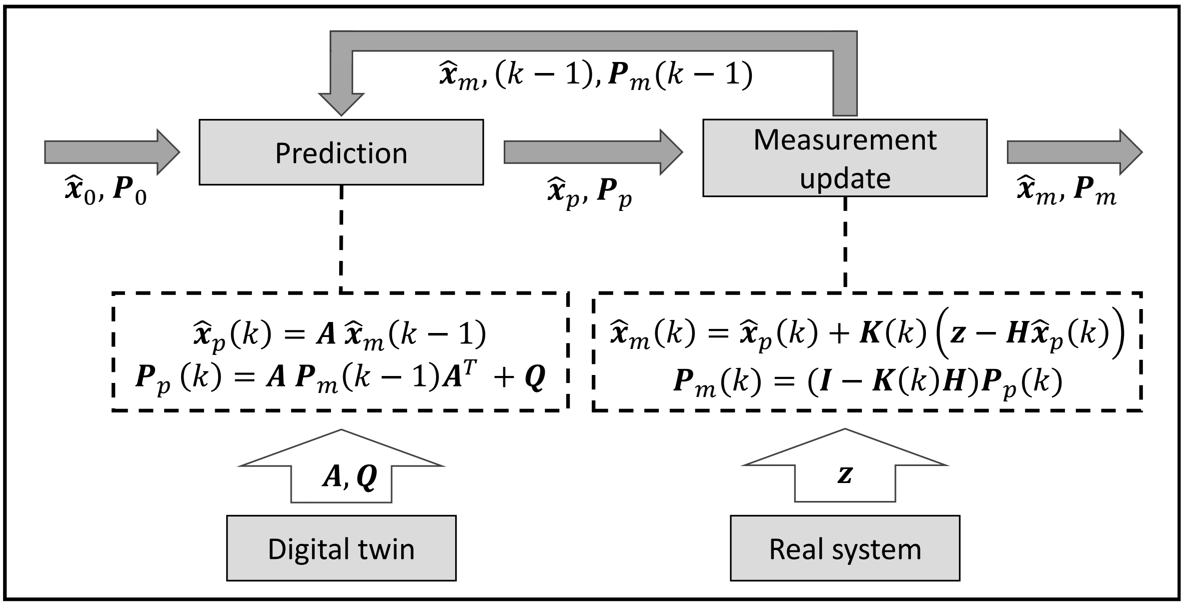


Figure 2: Overview of how the Kalman filter is used to estimate the systems thermal state **x** based on real world measurements **z**.

From here onwards, the notation $\hat{\mathbf{x}}$ is used to indicate the mean of a variable, whereas $\mathbf{P}$ is used to denote its corresponding covariance matrix. Moreover, the subscript $p$ will indicate the variables estimated during the prediction step as opposed to the subscript $m$ that distinguishes the variables estimated during the update step.

### 3.2. Prediction

$$\hat{\mathbf{x}}_p(k) = \mathbf{A} \cdot \hat{\mathbf{x}}_m(k-1) \tag{5}$$

$$\mathbf{P}_p(k) = \mathbf{A} \cdot \mathbf{P}_m(k-1) \cdot \mathbf{A}^T + \mathbf{Q} \tag{6}$$

During the first step, the value of the state and the corresponding covariance matrix are approximated: system dynamics are used to project the previous estimation forward into the future. The rationale of this first step is to obtain an estimation of the states' mean and variance by leveraging the a priori conditional probability density function, as explained in [33]: $p = p(\mathbf{x}(k)\,\mathbf{z}(1:k-1))$. On top of this concept, Equation 5 is derived: the mean state value and variance at the current time step is estimated, adopting only the system dynamics and associated process noise variance.

### 3.3. Measurement update

$$\mathbf{K}(k) = \mathbf{P}_p(k) \cdot \mathbf{H}^T \cdot (H \cdot\ \mathbf{P}_p(k) \cdot \mathbf{H}^T + \mathbf{R})^{-1} \tag{7}$$

$$\hat{\mathbf{x}}_m(k) = \hat{\mathbf{x}}_p(k) + \mathbf{K}(k) \cdot (\mathbf{z}(k) - \mathbf{H} \cdot \hat{\mathbf{x}}_p(k)) \tag{8}$$

$$\mathbf{P}_m(k) = (\mathbf{I} - \mathbf{K}(k) \cdot \mathbf{H}) \cdot \mathbf{P}_p(k) \tag{9}$$

In the second step, the states mean values are corrected with sensor measurements of physical variables **z**. Not all installed sensors are used in this step, only those chosen by the input selection described in Subsection 2.3 are used and called observed. The remaining installed temperature sensors are not used in the Kalman filter model but kept for validation of the model prediction. By applying the a priori probability density function and Bayes theorem, an equation for the posteriori conditional probability density function can be derived [33]: $p = p(\mathbf{x}(k)\ \mathbf{z}(1{:}k))$.
This concept is used to achieve an update equation formulation for the mean state value and associated variance. In Equation 7, the Kalman gain **K** is obtained by minimizing the a posteriori covariance. In Equation 8, **K** allows to scale the difference between predicted state and measured value, also called measurement innovation or the residual. The covariance is updated by adopting the Kalman gain as well (see Equation 9).

### 3.4. Stabilizability and Observability

Kalman filter operates optimally when the underlying dynamic system is linear and affected by Gaussian noise [19].
Additionally, if the convergence of the estimation error variance is guaranteed, it follows that the Kalman filter can effectively estimate every state of the LTI system. To assert error variance convergence, stabilizability and observability properties of the system must be analyzed.
Firstly, $(\mathbf{A}, \mathbf{H})$ should be fully observable. This requires that the matrix $\begin{matrix}\mathbf{A}-\lambda\mathbf{I}\\ \mathbf{H}\end{matrix}$ must have full rank for all eigenvalues $\lambda\ \geq 1$.

Secondly, the pair $(\mathbf{A}, \mathbf{G})$ where $\mathbf{Q} = \mathbf{G}\mathbf{G}^T$ (Cholesky factorization) must be stabilizable. Stabilizability of the matrix pair is ensured if $\begin{bmatrix} \mathbf{A} - \lambda\mathbf{I} \\ \mathbf{G} \end{bmatrix}$ has full rank. This is true for every positive definite $\mathbf{Q}$, and stabilizability is guaranteed. By ensuring the stabilizability, no excitements of unstable states by process noise is to be expected during the estimation.

Guaranteeing both the previous listed properties together is equivalent to stating that the estimated variance $\mathbf{P}_p(k)$ converges for every initial $\mathbf{P}_0$ to the steady state $\mathbf{P}_\infty$ as $k \to \infty$. $\mathbf{P}_\infty$ is in this case the unique positive semi-definite solution to the discrete Riccati equation (DARE) [8].

### 3.5. Noise covariance estimation

Effectively capturing a good estimation for process noise covariance is crucial for the Kalman filter to work properly. In order to approximate $\mathbf{Q}$, thermal states are derived from simulations with the reduced order FE model. A lowpass filter is then applied on the simulated state data in order to limit external excitation being considered as process noise. By comparing the simulation state data with the updated state values approximated using system dynamics, an estimation for the process noise covariance matrix is derived. The obtained process noise covariance matrix $\mathbf{Q}$ is also replaced by its discrete equivalent as it is estimated from the continuous system described in subsection 2.2 $\mathbf{Q}_d = \int_0^{T_s} e^{\mathbf{A}\tau}\mathbf{G}\mathbf{Q}_n\mathbf{G}^T e^{\mathbf{A}^T\tau} d\tau$

The process noise encloses many different forms of uncertainty surrounding the general model description such as material properties, the model order reduction and small disturbances of the process itself, e.g. changes in the airflow impacting the convective heat transfer coefficient.

The sensor noise covariance matrix $\mathbf{R}$ was obtained from the measurement uncertainty of all sensors.

## 4. Experimental setup

The developed Kalman filter-based compensation is exemplarily applied to predict the thermal errors of a demonstrator in the form of a thermal test bench as well as a 5-axis MT.

### 4.1. Thermal test bench

Figure 3 shows the FE model of the thermal test bench with each temperature sensor highlighted as a green area and the corresponding number. In total 40 temperature sensors are available as measurements on the physical test bench and have corresponding representation in the FE model. Further temperature sensors measuring for example the ambient temperature cannot be used as they currently have no representation in the FE model. For the temperature measurement, both type-K thermocouples and resistance temperature detectors (RTD) Pt100 elements are used with a sampling rate of 0.4 $Hz$. The temperature sensors are placed manually according to engineering knowledge, estimating that all relevant thermal effects can be ob-

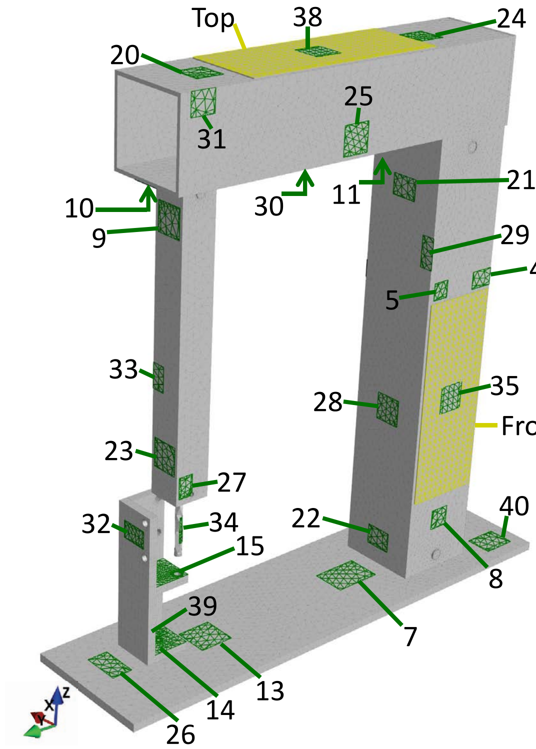

(a) Front view of the thermal test bench FE model.

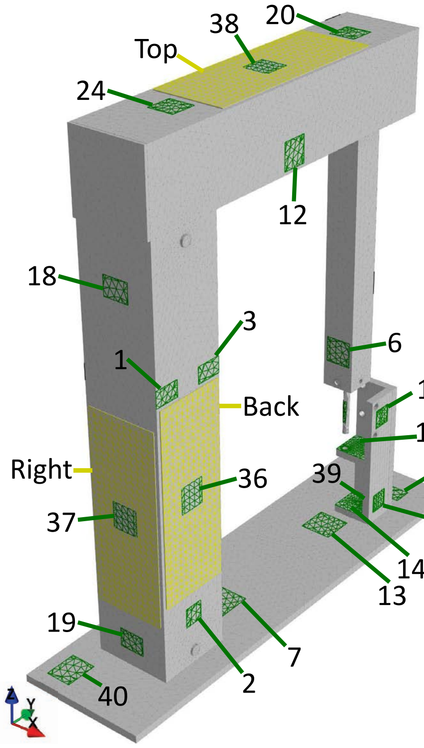

(b) Rear view of the thermal test bench FE model.

Figure 3: The thermal test bench FE mesh is shown from a front and rear view. It consists of three hollow structural aluminum parts, a base plate and the displacement probe holder. Four heat pads are labeled and highlighted by yellow areas. Temperature sensor locations are highlighted in green and labeled with a number. The average temperature of the green area is compared to the physical temperature sensor mounted in the center of this location.

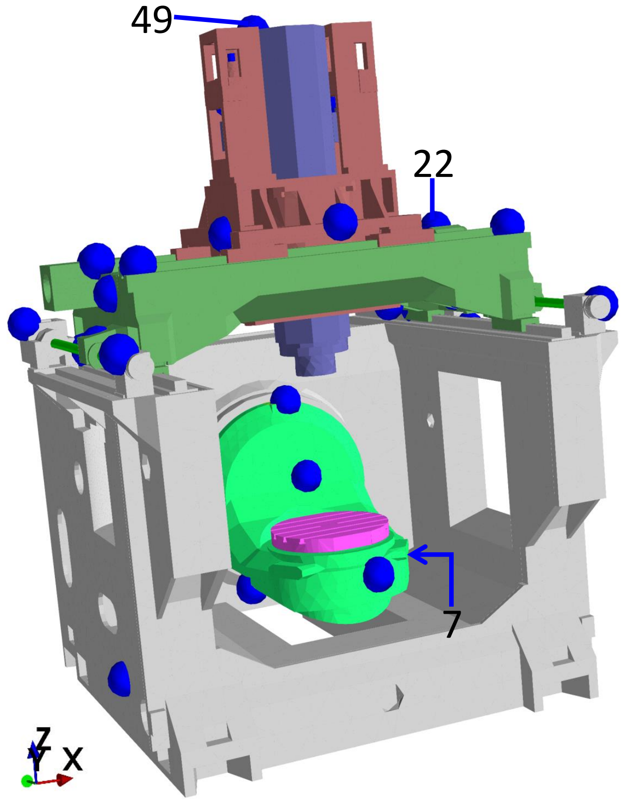


(a) Front view of the 5-axis MT FE model.

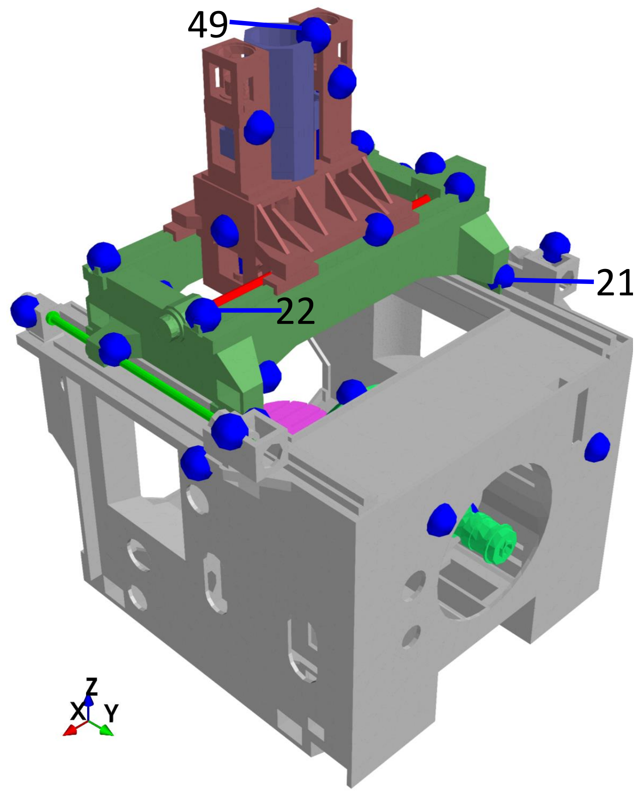


(b) Rear view of the 5-axis MT FE model.

Figure 4: Temperature sensor locations of the 5-axis machine tool are highlighted as blue spheres. The temperature sensors and numbers of Figure 8 are shown where they are used as not observed sensors for validation.

served. They are mounted thermally conductive on the structure and isolated against the air-side.

Four heating mats with a rated power of 65 $W$ excite the system (marked in yellow in Figure 3). First, each heat pad is activated individually for six hours, followed by a cooling down period of ten hours without any active heat source. After the heat pad on the top, right, back, and front are activated and deactivated in this order, all heating mats are activated simultaneously, followed by a cool-down period. In order to measure the thermal errors, the standardized test setup according to ISO 230-3:2020 [14] is employed. The thermally induced displacement is investigated between the tool at the end of the spindle and the probe holder representing the workpiece. For this purpose, five incremental displacement sensors (Heidenhain Specto ST1288, rated accuracy 1 $\mu m$) are used and measure with a frequency of 0.8 $Hz$. These are mounted at the probe holder with one measuring the Z expansion, two the X expansion one down at the spindle tip and one higher and two measuring the Y expansion at the same height as those for X. The structure is inspired by a C-frame of a MT and constructed from aluminum to achieve a fast-reacting demonstrator of an MT [36]. The whole setup is encased in a housing to reduce the air exchange with the ambient room and represent the housing of the working space of a real MT.

### 4.2. 5-axis MT NMV5000

To demonstrate the applicability of the developed method for real-world production machines, it is also successfully applied to a Mori Seiki NMV5000 DCG. This 5-axis MT has the following kinematic chain according to ISO 10791-1:2015 [16]: $V[w-C\ -B\ -b-[Y1,Y2]–X–[Z1,Z2]–(C)-t]$. The C-axis can be used at a maximum speed of 1200 rpm due to the turning option installed. Therefore, the C-axis also has a dedicated cooling circuit. The standard cooling circuit used to temper the rest of the MT.

The temperature sensors mounted on the structure, also represented in the FE model, are shown in Figure 4. Similar to the approach described in Subsection 4.1, 25 Pt100 RTD sensors are mounted according to engineering knowledge close to all relevant heat sources and along the structure. In order to measure the thermal error, a precision sphere is mounted on the table of the MT and a discrete R-Test is carried out at four different locations in the working space. To measure the relative position between the tool and the workpiece, a Renishaw OMP 60 touch trigger probe is used, and the first measurement is defined as the reference state. The measured axis-specific errors $E_{X0C}$, $E_{Y0C}$, $E_{Z0T}$, $E_{R0T}$, $E_{A0C}$, $E_{B0C}$, $E_{C0C}$, have a repeatability of 0.6 $\mu m$ and 3 $\mu m/m$ for $k = 2$ respectively, as shown by Blaser et al. [4]. These axis specific errors are then aggregated

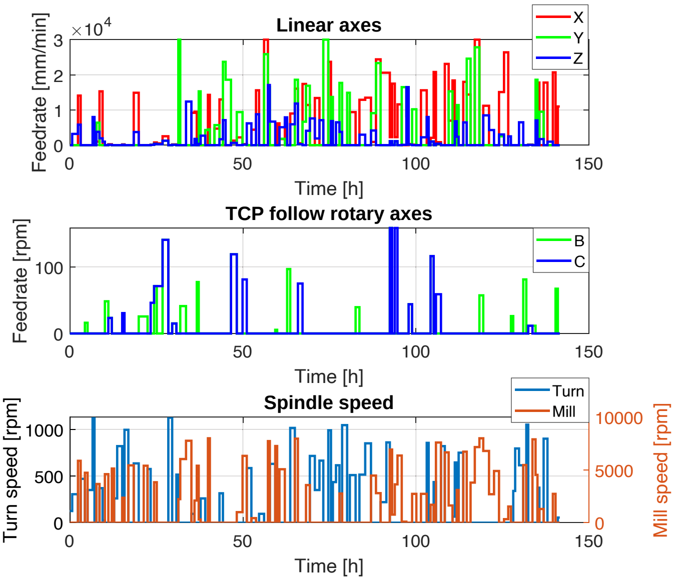


Figure 5: Speed profile of the linear and indexed rotary axes, as well as the milling and turning spindle of the long-term measurement on the 5-axis MT if the C-axis is in turning mode.

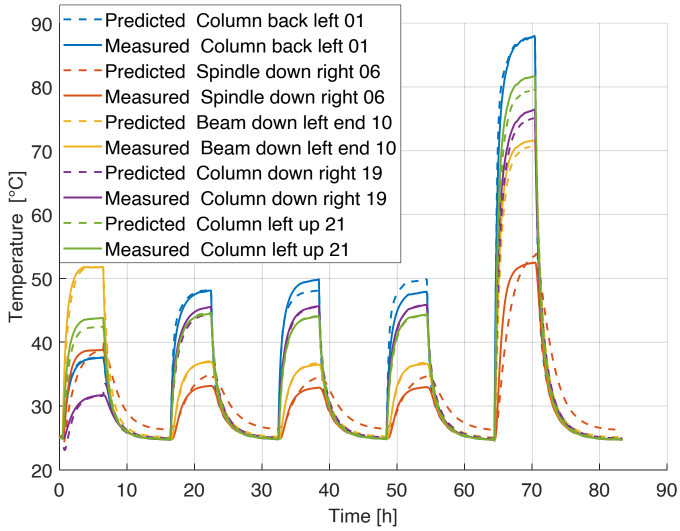


Figure 6: Temperature sensor measurements and model predictions for different temperature sensors, not used in the Kalman model as measurements, of the thermal test bench.

to the volumetric error in X,Y and Z direction, which is generated in the same manner as from the simulation model to allow comparability.

Figure 5 shows the load case applied to the 5-axis MT. After five minutes of axis movement at varying speeds, the load is interrupted by the measurement cycle using the touch probe, which is then followed by the next load case. Random axes movements are used to introduce thermal excitations in the system and emulate a varying production profile. Either all linear axes move in varying combinations, or the rotary axes are used in TCP follow mode. In that case X and Z follow the rotation of the B-axis, and X and Y follow the C-axis, respectively. Furthermore, the milling and turning spindle are used; the turning spindle is a specific mode of the C-axis that is not indexable but allows rotations up to 1200 rpm (which cannot be used in parallel to the rotary axes load cases, as B has to be clamped and C cannot be indexed) whereas the milling spindle can be used in parallel to all load cases except the C-axis in turning mode.

## 5. Results

In order to evaluate the performance of the developed Kalman filter based digital twin, the method is applied to long term measurements of both the thermal test bench as well as the 5-axis MT.

### 5.1. Compensation results of the thermal test bench

The difference between the prediction and measurement is quantified using the root mean squared error (RMSE).

$$RMSE = \sqrt{\frac{\sum_{i=1}^{N}(x_{i,meas} - \hat{x}_{i,predict})^2}{N}} \tag{10}$$

This weighs larger errors slightly more, as those are more relevant during the production process compared to smaller deviations. Another relevant metric is the peak to peak error (P2P), which is the maximal difference between the measured and simulated deformation. This represents the worst case thermally induced deviation and is very sensitive as it is only dependent on the largest modeling error which indicates the worst case during production that could be experienced.

$$Reduction = 1 - \frac{\text{RMSE}_{\text{after pred.}}}{\text{RMSE}_{\text{before pred.}}} \tag{11}$$

The model accuracy can be described by calculating the *Reduction* which is the residual RMSE over the original RMSE (which is based on a constant prediction of the initial value). Figure 6 shows five out of the 40 temperature measurements and the associated prediction from the digital twin. It can be noted that some differences between the prediction and measurement affect the magnitude and, to a lesser extent, the dynamic behavior such as the time constant of the temperatures. This might be caused by inaccuracies in the underlying system model. Overall, the RMSE of the unobserved temperatures is 2.7 $°C$. This corresponds to the RMSE of every sensors RMSE, which in this case are 24 unobserved temperature sensors. If a constant temperature of 25 $°C$ is compared to the measured temperatures the RMSE of all (unobserved) temperature sensors, this results in 16 $°C$ due to the large temperature range of the system which reaches more than 90 $°C$, if all heating mats are activated at the same time. Therefore more than 83% of the thermal behavior is explained by the temperature field reconstructed from the Kalman filter, which is deemed sufficient considering that no calibration is used.

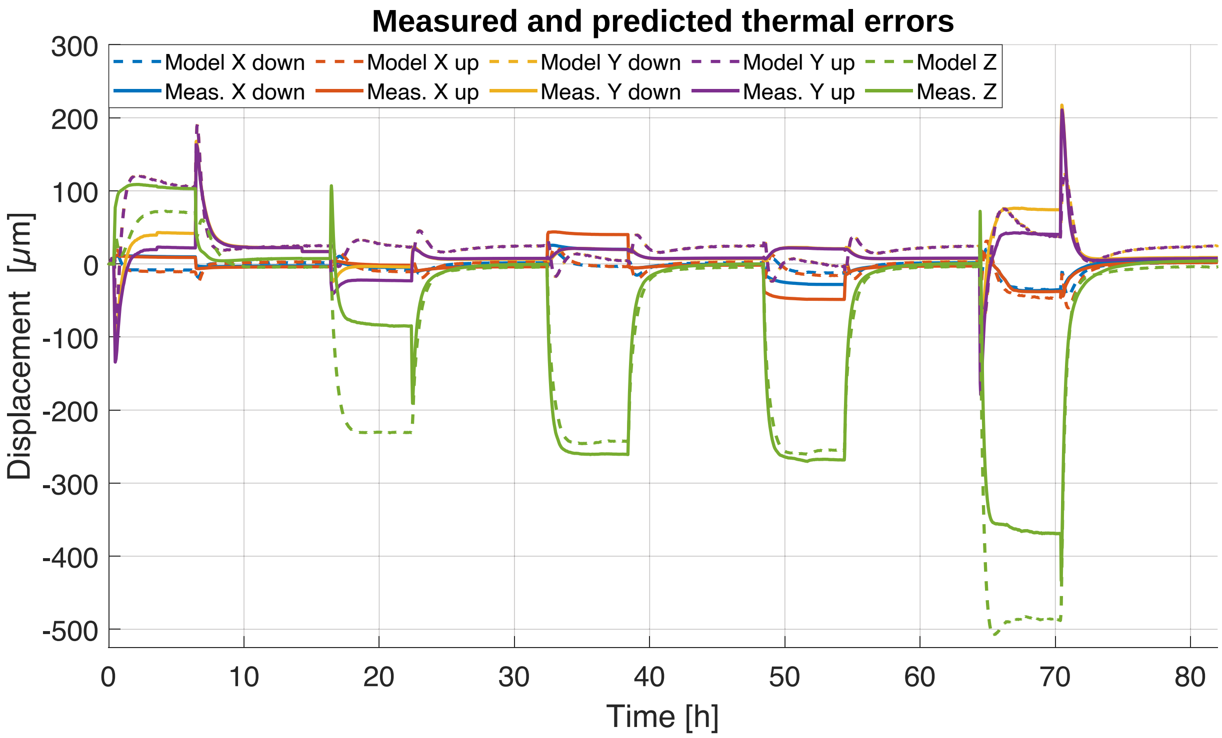


Figure 7: Thermal errors for the 5 measured displacement probes and the prediction values generated by solving the thermomechanical model using the Kalman filter corrected thermal state.

Figure 7 shows the thermal error that was either measured or calculated based on the temperature state estimated before for all five incremental displacement probes. Table 2 shows the RMSE and P2P values for all errors. The Z direction is by far the most dominant and, therefore, also shows the highest model performance with reductions for both metrics above 60%. The X direction is the least significant as it represents the symmetry plane and therefore is only significant when an asymmetric head load is applied.

One reason for modeling error, especially on the second load case, is the way the heat mat on the right side is mounted. While the front and back sides are glued directly from the heat mat to the structure, the right side consists of the heat mat on a movable aluminum plate fixed with screws. Therefore, the contact between the structure and heat mat is not ideal leading to an irregular (and changing due to the thermal load) airgap between part of the structure and heat mat. This is not included in the model and one possible source for the especially pronounced error during this load case. This shows that real irregularities that cannot easily be considered in the underlying model of the digital twin poses a source of errors that in certain conditions lead to a poor model performance. Therefore a high model fidelity is desirable and a repeatable real system crucial.

### 5.2. Compensation results of the 5-axis MT

In order to show that the previous results are also applicable to real-world production machines the aforementioned NMV5000 5-axis MT is used as a demonstrator as well.

Table 2: The difference of the measured thermal error compared to the residual error (Resid.) of the prediction compared to the measurement and percentage reduction. The RMSE (root mean squared error) is an indicator for the average thermal error. The peak to peak (P2P) values represent the maximal deviation of the measurement and after correction.

| | RMSE | | | Peak to Peak | | |
|---|---|---|---|---|---|---|
| **Sensor** | **Meas. [$\mu$m]** | **Resid. [$\mu$m]** | **Red. %** | **Meas. [$\mu$m]** | **Resid. [$\mu$m]** | **Red. %** |
| **X Up** | 13.2 | 10 | 24.2 | 65.5 | 68.6 | -5.2 |
| **X Down** | 19.5 | 16.9 | 13.2 | 92.5 | 105.28 | -13.9 |
| **Y Up** | 31.9 | 27 | 15.3 | 365.6 | 245.7 | 32.8 |
| **Y Down** | 28.1 | 32.2 | -14.6 | 389.4 | 265.6 | 31.2 |
| **Z** | 142.6 | 54.1 | 62.1 | 542.3 | 197.8 | 63.5 |

Figure 8 shows temperatures measured and predicted of the 5-axis MT. 13 sensors were observed out of 25, the remaining were reconstructed from the temperature field prediction for validation. The RMSE for all twelve unobserved temperature sensors is 1.3 °$C$.

Figure 9 shows the volumetric thermal error in the X,Y and Z directions. As X is the symmetry plane of the MT it is the lowest in magnitude while Y and Z are varying around 40 $\mu m$ each. The observed prediction aligns well but not perfectly with the thermal error. Nonetheless, the precision of the model is constrained due to incomplete observability, which was given in the case of the thermal test bench, as it was not yet feasible to equip all moving components with temperature sensors. To enhance the model's accuracy and reach the level attainable through state of the art data-driven approaches, assuming the

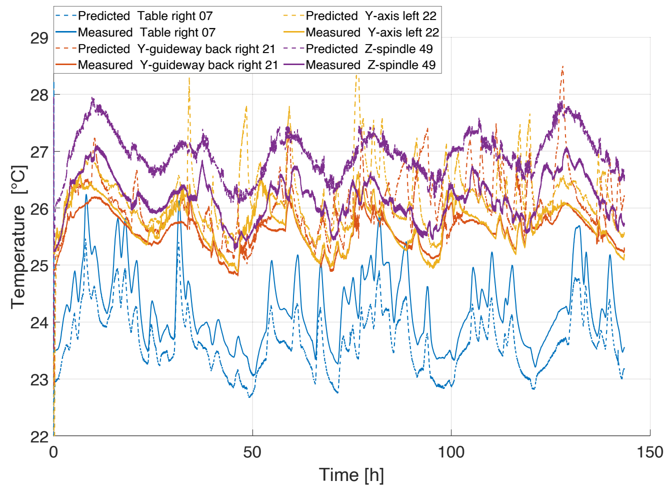


Figure 8: Temperature sensor measurements and model predictions for different temperature sensors, not used in the kalman model as measurements, of the 5-axis MT.

training data is representative, further improvements are necessary in both the model's representation, such as adopting variable model parameters in for example the convective heat transfer coefficients, and in the optimal sensor positioning.

## 6. Conclusion

The introduced Kalman filter can, combined with model order reduced FE models, effectively reconstruct the entire thermal field, which allows the mechanical model to be evaluated. This enables prediction and subsequent compensation of the thermal errors for machine tools in real-time without the need for experimental training data. The used number of sensors is 16 in the case of the thermal test bench, and 13 in the case of the 5-axis MT, which is a reduction by more than an order of magnitude compared to previous work by Kizaki et al. [20], who used 284 temperature sensors and linear interpolation instead of a Kalman filter coupled with a thermal system model as proposed in this work.

The entire temperature field can be reconstructed accurately using the adaptive Kalman filter and discrete temperature sensor measurements. This leads to average deviations for the unobserved temperature sensors of only 2.7 $°C$ for the thermal test bench and 1.3 $°C$ for a 5-axis MT. This approach enables the use of only 16 temperature sensors for the test bench and 13 sensors for the 5-axis Machine Tool (MT) to accurately represent systems with 200,000 to 350,000 mesh elements, respectively. This demonstrates its wide applicability for real-time monitoring of large-scale mechatronic thermomechanical systems. The mechanical evaluation of the thermal error also shows good agreement with the measurement by an average reduction of 52.7% of thermal error RMSE for the thermal test bench with no real-world calibration data used to fit this model.

The advantage of this approach is that no training data is required for compensation if a model can be parametrized and validated. Therefore, this is a promising option for a physics-based, real-time, capable thermal error compensation of machine tools, increasing production accuracy at no productivity loss and additional energy expenditure.

Future research will investigate the optimal placement of the temperature sensors to ensure ideal compensation at minimal sensor requirements and use of data from the MT control as virtual sensors improving observability. Another open field of research is further improving the underlying system model, especially regarding efficient parametrization of the boundary conditions. The physics-based approaches could also be used in parallel to data-driven approaches to realize a hybrid solution of physics and data-driven thermal error compensation, further improving the compensation accuracy.

## Declaration of Competing Interest

The authors declare that they have no known competing financial interests or personal relationships that could have appeared to influence the work reported in this paper.

## Acknowledgements

This work was co-financed by Innosuisse - Swiss Innovation Agency, Project no. 27835.1 IP-ENG. The MT provided by MTTRF is greatly appreciated. The authors wish to thank Prof. Stephen Duncan and Dr. Nico Zimmermann for the helpful discussions and their insights.

## References

[1] Abdulshahed, A.M., Longstaff, A.P., Fletcher, S., Myers, A., 2015. Thermal error modelling of machine tools based on ANFIS with fuzzy c-means clustering using a thermal imaging camera. Applied Mathematical Modelling 39, 1837–1852. doi:10.1016/j.apm.2014.10.016.

[2] Alsadik, B., 2019. Kalman Filter. Adjustment Models in 3D Geomatics and Computational Geophysics , 299–326doi:10.1016/b978-0-12-817588-0.00010-6.

[3] Auger, F., Hilairet, M., Guerrero, J.M., Monmasson, E., Orlowska-Kowalska, T., Katsura, S., 2013. Industrial applications of the kalman filter: A review. IEEE Transactions on Industrial Electronics 60, 5458–5471. doi:10.1109/TIE.2012.2236994.

[4] Blaser, P., Pavliček, F., Mori, K., Mayr, J., Weikert, S., Wegener, K., 2017. Adaptive learning control for thermal error compensation of 5-axis machine tools. Journal of Manufacturing Systems 44, 302–309.

[5] Bryan, J., 1990. International Status of Thermal Error Research (1990). CIRP Annals - Manufacturing Technology 39, 645–656. doi:10.1016/S0007-8506(07)63001-7.

[6] Chengyang, W., Sitong, X., Wansheng, X., 2021. Spindle thermal error prediction approach based on thermal infrared images: A deep learning method. Journal of Manufacturing Systems 59, 67–80. doi:10.1016/j.jmsy.2021.01.013.

[7] Czwartosz, R., Jedrzejewski, J., CZWARTOSZ, Robert, J.J., 2022. Application of machine learning in the precise and cost-effective self-compensation of the thermal errors of CNC machine tools–a review. Journal of Machine Engineering 22.

[8] Davis, M., 2013. Stochastic modelling and control. Springer Science & Business Media.

[9] Denkena, B., Abele, E., Brecher, C., Dittrich, M.A., Kara, S., Mori, M., 2020. Energy efficient machine tools. CIRP Annals 69, 646–667. doi:10.1016/j.cirp.2020.05.008.

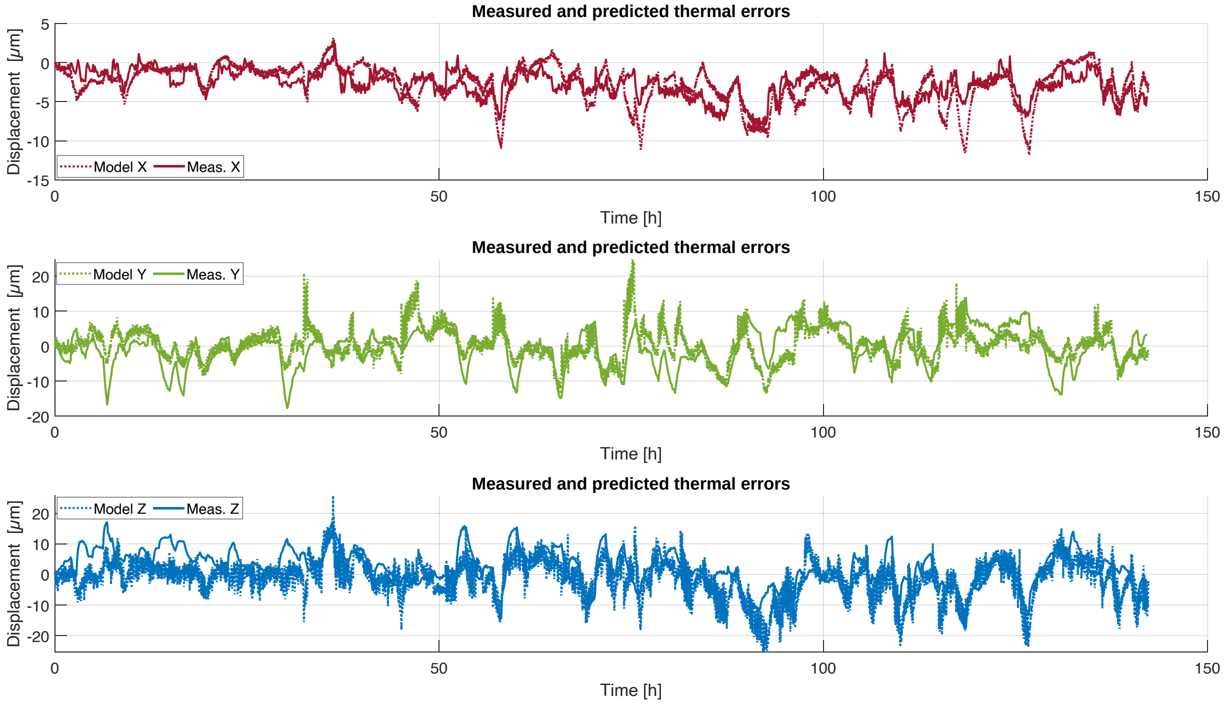


Figure 9: Thermal errors for the measured volumetric displacement in X-,Y- and Z-direction and the prediction values generated by solving the thermomechanical model using the Kalman filter corrected thermal state.


[10] Gomez-Acedo, E., Olarra, A., Orive, J., Lopez De La Calle, L.N., 2013. Methodology for the design of a thermal distortion compensation for large machine tools based in state-space representation with Kalman filter. International Journal of Machine Tools and Manufacture 75, 100–108. doi:10.1016/j.ijmachtools.2013.09.005.

[11] Guo, J., Li, B., Liu, Z., Hong, J., Zhou, Q., 2016. A new solution to the measurement process planning for machine tool assembly based on Kalman filter. Precision Engineering 43, 356–369. doi:10.1016/j.precisioneng.2015.08.016.

[12] Hernández-Becerro, P., Mayr, J., Wegener, K., Hernández Becerro, P., Mayr, J., Wegener, K., 2020. Efficient thermo-mechanical model of a precision 5-axis machine tool, in: Conference Proceedings on Thermal Issues 2020, euspen. p. TI20116. URL: www.euspen.eu.

[13] Hernández-Becerro, P., Purtschert, J., Konvicka, J., Buesser, C., Schranz, D., Mayr, J., Wegener, K., 2021. Reduced-Order Model of the Environmental Variation Error of a Precision Five-Axis Machine Tool. Journal of Manufacturing Science and Engineering, Transactions of the ASME 143. doi:10.1115/1.4047739.

[14] International Organization for Standardization (ISO), 2020. Test code for machine tools — Part 3: Determination of thermal effects. ISO 230-3:2020 .

[15] Irino, N., Kobayashi, A., Shinba, Y., Kawai, K., Spescha, D., Wegener, K., 2023. Digital twin based accuracy compensation. CIRP Annals 72, 345–348. doi:10.1016/j.cirp.2023.04.088.

[16] ISO 10791-1, 2015. Test conditions for machining centers – Part 1: Geometric tests for machines with horizontal spindle (horizontal Z-axis). ISO 10791-1:2015(E) .

[17] Kalman, R.E., 1960. A new approach to linear filtering and prediction problems. Journal of Fluids Engineering, Transactions of the ASME 82, 35–45. doi:10.1115/1.3662552.

[18] Kim, Y., Alcantara, D., Zohdi, T.I., 2022. Thermal state estimation of fused deposition modeling in additive manufacturing processes using Kalman filters. International Journal for Numerical Methods in Engineering 123, 3021–3033. doi:10.1002/nme.6490.

[19] Kim, Y., Bang, H., 2018. Introduction to Kalman filter and its applications. Introduction and Implementations of the Kalman Filter 1, 1–16.

[20] Kizaki, T., Tsujimura, S., Marukawa, Y., Morimoto, S., Kobayashi, H., 2021. Robust and accurate prediction of thermal error of machining centers under operations with cutting fluid supply. CIRP Annals 70, 1–4. doi:10.1016/j.cirp.2021.04.074.

[21] Lang, S., Zimmermann, N., Mayr, J., Wegener, K., Bambach, M., 2023. Thermal Error Compensation Models Utilizing the Power Consumption of Machine Tools, in: International Conference on Thermal Issues in Machine Tools, Springer. pp. 41–53.

[22] Liu, M., Fang, S., Dong, H., Xu, C., 2021. Review of digital twin about concepts, technologies, and industrial applications. Journal of Manufacturing Systems 58, 346–361. doi:10.1016/j.jmsy.2020.06.017.

[23] Mareš, M., Horejš, O., Havlík, L., 2020. Thermal error compensation of a 5-axis machine tool using indigenous temperature sensors and CNC integrated Python code validated with a machined test piece. Precision Engineering 66, 21–30.

[24] Mayr, J., Blaser, P., Ryser, A., Hernandez-Becerro, P., 2018. An adaptive self-learning compensation approach for thermal errors on 5-axis machine tools handling an arbitrary set of sample rates. CIRP Annals 67, 551–554.

[25] Mayr, J., Jedrzejewski, J., Uhlmann, E., Alkan Donmez, M., Knapp, W., Härtig, F., Wendt, K., Moriwaki, T., Shore, P., Schmitt, R., Brecher, C., Würz, T., Wegener, K., 2012. Thermal issues in machine tools. CIRP Annals 61, 771–791.

[26] Miao, E.M., Gong, Y.Y., Niu, P.C., Ji, C.Z., Chen, H.D., 2013. Robustness of thermal error compensation modeling models of CNC machine tools. International Journal of Advanced Manufacturing Technology 69, 2593–2603. doi:10.1007/s00170-013-5229-x.

[27] Middleton, R.H., Goodwin, G.C., 1990. Digital control and estimation: a unified approach. Prentice Hall Professional Technical Reference.

[28] Mori, K., Ogura, D., Matsubara, A., 2022. Energy-efficient manufacturing with indoor conditions offset considering weather conditions doi:10.1016/j.cirpj.2022.02.014.

[29] Pelleg, D., Moore, A.W., 2000. X-means: Extending k-means with efficient estimation of the number of clusters., in: Icml, pp. 727–734.

[30] Polotski, V., Kenne, J.P., Gharbi, A., 2020. Kalman filter based production control of a failure-prone single-machine single-product manufacturing system with imprecise demand and inventory information. Journal of Man-

ufacturing Systems 56, 558–572. doi:10.1016/j.jmsy.2020.07.010.
[31] Spescha, D., Weikert, S., Retka, S., Wegener, K., 2018. Krylov and Modal Subspace Based Model Order Reduction with A-Priori Error Estimation doi:10.3929/ethz-b-000284435.
[32] Spescha, D., Weikert, S., Wegener, K., 2020. Simulation in the Design of Machine Tools. Reinventing Mechatronics: Developing Future Directions for Mechatronics , 163–177.
[33] Welch, G., Bishop, G., 1995. An introduction to the Kalman filter .
[34] Zimmermann, N., Büchi, T., Mayr, J., Wegener, K., 2022a. Self-optimizing thermal error compensation models with adaptive inputs using Group-LASSO for ARX-models. Journal of Manufacturing Systems .
[35] Zimmermann, N., Lang, S., Blaser, P., Mayr, J., 2020. Adaptive input selection for thermal error compensation models. CIRP Annals 69, 485–488.
[36] Zimmermann, N., Mayr, J., Wegener, K., 2022b. An action-oriented teaching approach for intelligent and energy efficient precision manufacturing. Manufacturing Letters 33, 961–969. doi:10.1016/j.mfglet.2022.07.117.
[37] Zimmermann, N., Müller, E., Lang, S., Mayr, J., Wegener, K., 2023. Thermally compensated 5-axis machine tools evaluated with impeller machining tests. CIRP Journal of Manufacturing Science and Technology 46, 19–35. doi:10.1016/j.cirpj.2023.07.005.